



# Kinetics analysis of the reactions responsible for myoglobin chemical state in meat using an advanced reaction–diffusion model

A Kondjoyan, J. Sicard, M Badaroux, Philippe Gatellier

## ► To cite this version:

A Kondjoyan, J. Sicard, M Badaroux, Philippe Gatellier. Kinetics analysis of the reactions responsible for myoglobin chemical state in meat using an advanced reaction–diffusion model. Meat Science, 2022, 191, 10.1016/j.meatsci.2022.108866 . hal-03696487

HAL Id: hal-03696487

<https://hal.inrae.fr/hal-03696487>

Submitted on 16 Jun 2022

**HAL** is a multi-disciplinary open access archive for the deposit and dissemination of scientific research documents, whether they are published or not. The documents may come from teaching and research institutions in France or abroad, or from public or private research centers.

L'archive ouverte pluridisciplinaire **HAL**, est destinée au dépôt et à la diffusion de documents scientifiques de niveau recherche, publiés ou non, émanant des établissements d'enseignement et de recherche français ou étrangers, des laboratoires publics ou privés.



Distributed under a Creative Commons Attribution - NonCommercial - NoDerivatives 4.0 International License



## Kinetics analysis of the reactions responsible for myoglobin chemical state in meat using an advanced reaction–diffusion model

A. Kondjoyan<sup>a,\*</sup>, J. Sicard<sup>a</sup>, M. Badaroux<sup>b</sup>, P. Gatellier<sup>a</sup>

<sup>a</sup> INRAE, QuaPA, 63122 Saint-Genès-Champanelle, France

<sup>b</sup> ISIMA, Clermont Auvergne INP, Université Clermont-Auvergne, 63178 Aubière, France



### ARTICLE INFO

**Keywords:**

Beef  
Simulation  
Prediction  
Biochemistry  
Preservation  
Oxygen

### ABSTRACT

Here we developed an advanced reaction–diffusion model to predict the evolution of the myoglobin state in beef meat using numerous reactions with rate constants of different orders of magnitude. The initial scheme included 44 reactions from the literature. Sensitivity analysis proved that this initial scheme was equivalent to a simple 22-reaction scheme. Results calculated with this scheme were compared against the spatial distributions of oxy-myoglobin ( $\text{MbO}_2$ ), metmyoglobin (MMb) and deoxymyoglobin (DMb) measured in meat cuts stored at 20°C under air-permeable packaging. We found global agreement between measured and calculated distributions when adequate rate constant values were used, particularly for the formation of  $\text{MbO}_2$  from DMb. The model was used to calculate evolutions in  $\text{MbO}_2$  and MMb distributions under different situations (modified-atmosphere packaging, Fenton chemistry with or without water-soluble antioxidants, increased mitochondrial oxygen consumption). Results were used to discuss the underlying kinetics reaction mechanisms and the performances and limits of the model.

### 1. Introduction

Most beef meat remains sold fresh. Color is a major factor in consumer rejection of beef meat cuts, which leads to an estimated 3–4% of total meat output going to waste (Cucci, N'Gatta, Sanguansuk, Lebert, & Audonnet, 2020). Research estimates that a 3.5% loss of beef meat at supermarket retail equates to 29% of the overall supermarket food loss when translated into carbon footprint (Eriksson, Strid, & Hansson, 2014). The color of red meat comes from myoglobin, a water-soluble protein that stores oxygen in the muscles of living animals. Red meat color is related to heme iron oxidation and the binding of oxygen to globin. In fresh meat that has not been exposed to carbon monoxide, myoglobin is mainly found in three forms: deoxymyoglobin, oxy-myoglobin, and metmyoglobin, which are abbreviated here as DMb/ $\text{MbFe}^{2+}$ ,  $\text{MbO}_2/\text{MbFe}^{2+}(\text{O}_2)$  and MMb/ $\text{MbFe}^{3+}$ , respectively. DMb leads to purplish,  $\text{MbO}_2$  to bright red, and MMb to brown beef meat color. Consumers look for bright red-color meat and reject brown-color meat. Over the course of animal slaughter, meat cutting and storage, the myoglobin changes between these myoglobin forms. The most recent studies have been reviewed by Ramanathan et al. (2020). Myoglobin state can theoretically be predicted using reaction–diffusion models.

Extremely simple reaction–diffusion models have been proposed in the past. Toftekskov, Hansen, and Bailey (2017) recently developed a more comprehensive numerical model to predict meat preservation under modified-atmosphere packaging (MAP). Even if this model marks significant progress compared to previous studies, it is still not able to correctly simulate experimental results. There are two main reasons for this: (1) the reaction model remains simplistic compared to the knowledge available in the biochemical literature, and (2) the model does not fully consider the coupling between oxygen diffusion and reactions kinetics. These limitations are probably due to the difficulty in developing—and then optimizing—a coupled reaction–diffusion model that is able to consider complex reaction routes.

This paper aims to go further than Toftekskov et al. (2017) by better integrating key biochemical science and by quantifying the impact of the different reactions proposed in literature on the kinetics of formation of  $\text{MbO}_2$ , MMb and DMb. This ‘no a priori’ approach (no preliminary simplification without a numerical sensitivity analysis of the system) will bring a better understanding of how different groups of reactions contribute to the variation in the state of myoglobin. Our initial reaction scheme essentially features 3 different groups of reactions. The first group of reactions concerns variations in the forms of myoglobin due to

\* Corresponding author.

E-mail address: [alain.kondjoyan@inrae.fr](mailto:alain.kondjoyan@inrae.fr) (A. Kondjoyan).

oxygen and related compounds ( $\text{H}_2\text{O}_2$ ,  $\text{HO}_2^\circ/\text{O}_2^\circ$ ). Associated with this group are the reactions related to oxygen consumption by mitochondrial respiration and the production of hydrogen peroxide by glycolysis. The second group of reactions consists of the Fenton reactions driven by non-heme iron found in the meat. The third group of reactions consists of the reactions connected with the water-soluble antioxidants found in meat, i.e. superoxide dismutase, catalase, carnosine, glutathione, and ascorbate. The complete list of the 33 reactions of these two last groups is not detailed in this paper. They come directly from our previous study on Fenton chemistry in a liquid meat-mimetic medium (Queslati, Promeyrat, Gatellier, Daudin, & Kondjoyan, 2018). Thus, the following deals with the reactions of the first group. In this first group, the analysis of the literature found 9 reactions directly involving myoglobin (reactions 1–9, Table 1). The literature gives two routes to the formation of MMb. The first route is the classical autoxidation reaction that forms MMb from  $\text{MbO}_2$  (reaction 1, Table 1), while the second route is the route proposed by Brantley, Smerdon, Wilkinson, Singleton, and Olson (1993) which starts from DMb to form MMb (reactions 4–6, Table 1). In the first route, the autoxidation reaction (reaction 1, Table 1) is a proton-assisted that, in beef meat (pH 5.5), mainly leads to the formation of  $\text{O}_2^\circ$  (pKa of  $\text{HO}_2^\circ/\text{O}_2^\circ$  about 5.0). The oxygenation reaction (reaction 3, Table 1) is known to be extremely fast, in living animals it responds to the physiological need to rapidly store the oxygen transported by the blood in muscles. In the second route, MMb is formed directly from DMb. In the mechanism proposed by Brantley et al. (1993), a nucleophile named N binds to DMb to facilitate the oxidation of DMb to MMb. It is unclear how N is connected to the protons present in water or to the water molecule itself. Reaction mechanisms of myoglobin with  $\text{H}_2\text{O}_2$  that lead to the formation of ferrylmyoglobin from MMb has been observed (Gatellier, Anton, & Renerre, 1995) and reviewed (Richards, 2013), and a feedback reaction from ferrylmyoglobin to MMb is also observed (reactions 7–9, Table 1).

After slaughter, mitochondrial respiration in muscles stops as soon as the oxygen has been consumed, but some mitochondria survive and remain able to consume oxygen even 60 days after slaughter, as shown when a beef heart muscle is stored under vacuum at 4°C (Cheah & Cheah, 1971). Numerous publications have analyzed the postmortem respiration of muscles (Cheah & Cheah, 1971; England et al., 2018; Ke et al., 2017; Mancini, Belskie, Suman, & Ramanathan, 2018; Renerre & Labas, 1987; Tang et al., 2005), and most of them have been reviewed (Ramanathan & Mancini, 2018). Oxygen consumption rate (OCR) depends on the amount and physiological state of the mitochondria as well as on the pH and the richness of the substrate in the molecules involved in the tricarboxylic acid (TCA, or Krebs) cycle. The ability of mitochondria to consume  $\text{O}_2$  varies also over time as their membrane degrades due to lipid oxidation, leading to their death (Tang et al., 2005).

This paper analyzes the effect of reaction-diffusion mechanisms on the kinetics of variation of the state of myoglobin in a piece of meat subjected to different oxygen concentrations. DFD (Dark Firm and Dried) beef meat, with high ultimate pH, is always much darker than normal ultimate pH meat. Krzywicki (1979) has shown that the color of the DFD meat can be influenced by light scattering properties whereas this was not the case for meat at normal ultimate pH. In the present paper, only meat at normal ultimate pH, about 5.6, is considered. The proportions of the different forms of myoglobin are often determined in meat extracts by spectrophotometric methods. Since the work of Stewart, Zipser, and Watts (1965), several methods have been used to determine these proportions and Tang, Faustman, and Hoagland (2004) have modified Krzywicki's equations, to determine the proportions of MMb, DMb, and  $\text{MbO}_2$ , considering wavelength maxima at 503, 557, and 582 nm, respectively. In this paper, the model calculations will be compared against the spatial distributions of the different forms of myoglobin measured by Saenz, Hernandez, Alberdi, Alfonso, and Manuel Dineiro (2008) in a meat cut stored at 20°C. These data were selected from literature because they give the opportunity to go further in the validation of the mathematical model, and in the discussion of the

**Table 1**

Scheme of the 23 reactions retained after sensitivity analysis performed in the homogeneous oxygen medium. With reaction 9 neglected, 22 of these reactions were introduced in the reaction-diffusion model to predict the evolution of myoglobin in the meat tissue.

No.	Reaction	Rate constant, k pH = 5.5, T = 20°C		Reference
		Initial literature value	Final model value	
1	$\text{MbFe}^{2+}(\text{O}_2) \rightarrow \text{MbFe}^{3+} + \text{HO}_2^\circ/\text{O}_2^-$	$6.4 \times 10^{-6}$	$6.4 \times 10^{-8}$	Tofteskov et al., 2017
2	$\text{MbFe}^{2+}(\text{O}_2) \rightarrow \text{MbFe}^{2+} + \text{O}_2$	$2.0 \times 10^1$ to $4.0 \times 10^2$	$2.4 \times 10^{+1}$ $1.0 \times 10^8$	Richards, 2013
3	$\text{MbFe}^{2+} + \text{O}_2 \rightarrow \text{MbFe}^{2+}(\text{O}_2)$	$2.0 \times 10^5$ to $4.0 \times 10^8$	with $N = 2$ $2.0 \times 10^8$ with $N = 3$	Brantley et al., 1993
4	$\text{MbFe}^{2+} + \text{N} \rightarrow \text{MbNFe}^{2+}$	$1.0 \times 10^{-2}$ $N = 1$ to 45	$1.0 \times 10^{-2}$ $N = 2$ to 3	Tofteskov et al., 2017
5	$\text{MbNFe}^{2+} \rightarrow \text{MbFe}^{2+} + \text{N}$	$3.3 \times 10^{-5}$	$3.3 \times 10^{-5}$	Richards, 2013
6	$\text{MbNFe}^{2+} + \text{O}_2 \rightarrow \text{MbNFe}^{3+} + \text{O}_2^-$	$5.0 \times 10^{-1}$	$5.0 \times 10^{-1}$	Brantley et al., 1993
7	$\text{MbFe}^{3+} + \frac{3}{2}\text{H}_2\text{O}_2 + \text{H}^+ \rightarrow \text{Mb}^+\text{Fe}^{4+} = \text{O} + 2\text{H}_2\text{O}$	$2.5 \times 10^4$	Small effect compared to 8	Richards, 2013
8	$\text{MbFe}^{3+} + \frac{3}{2}\text{H}_2\text{O}_2 \rightarrow \text{MbFe}^{4+} = \text{O} + \text{H}_2\text{O} + \text{HO}^-$ $\text{MbFe}^{4+} = \text{O} + \text{H}_2\text{O} \rightarrow$	$5.1 \times 10^1$	$5.1 \times 10^1$	Richards, 2013
9	$\text{MbFe}^{3+} + \frac{1}{2}\text{H}_2\text{O}_2 + \frac{1}{2}\text{O}_2 + \text{H}^+ \rightarrow \text{Glc} + 6\text{O}_2 + 38\text{ADP} + 38\text{PO}_4^{2-} + 32\text{H}^+ \rightarrow 6\text{HCO}_3^- + 38\text{H}_2\text{O} + 38\text{ATP}$	$1.2 \times 10^{-7}$	Can be neglected	Gatellier et al., 1995
10	$\text{Simplified by a zero or first-order reaction}$ $\text{Glc} + n\text{H}_2\text{O} + \sum m_i X_i \rightarrow p$ $\text{H}_2\text{O}_2 + \sum q_i Y_i$	First-order reaction and $1.2 \times 10^{-7}$	First-order reaction and $1.2 \times 10^{-7}$	See Table 3
11	$\text{Simplified by a first-order reaction}$ $\text{Fe}^{2+} + \text{H}_2\text{O}_2 \rightarrow \text{Fe}^{3+} + \text{HO}^- + \text{HO}^\circ$ $\text{Fe}^{3+} + \text{H}_2\text{O}_2 \rightarrow \text{Fe}^{2+} + (\text{HO}_2^\circ/\text{O}_2^-) + \text{H}^+$ $\text{Fe}^{2+} + (\text{HO}_2^\circ/\text{O}_2^-) \rightarrow \text{Fe}^{3+} + \text{H}_2\text{O}_2$ $\text{Fe}^{3+} + (\text{HO}_2^\circ/\text{O}_2^-) \rightarrow \text{Fe}^{2+} + \text{O}_2 + \text{H}^+$ $\text{Fe}^{2+} + \text{O}_2 \rightarrow \text{Fe}^{3+} + (\text{HO}_2^\circ/\text{O}_2^-)$	$1.25 \times 10^{-8}$	$1.25 \times 10^{-8}$	
12	$\text{H}_2\text{O}_2 + \text{catalase} \rightarrow \frac{1}{2}\text{O}_2 + \text{H}_2\text{O}$	$10^7$	$10^7$	
18	$\text{carnosine} + (\text{HO}_2^\circ/\text{O}_2^-) \rightarrow \text{lost compound 1}$	$8.3 \times 10^4$	$8.3 \times 10^4$	Oueslati et al., 2018
19	$\text{carnosine} + \text{HO}^\circ \rightarrow \text{lost compound 2}$	$9 \times 10^9$	$9 \times 10^9$	
20	$(\text{AH}_2/\text{AH}^-) + \text{Fe(III)} \rightarrow (\text{AH}^\circ/\text{A}^\circ) + \text{Fe(II)}$ $(\text{AH}_2/\text{AH}^-) + (\text{HO}_2^\circ/\text{O}_2^-) + \text{H}^+ \rightarrow (\text{AH}_2/\text{AH}^-) + \text{HO}_2^\circ/\text{O}_2^-$	$10$	$10$	
21	$\text{O}_2^\circ + \text{H}^+ \rightarrow (\text{AH}^\circ/\text{A}^\circ) + \text{H}_2\text{O}_2$	$10^6$	$10^6$	
22	$2(\text{AH}^\circ/\text{A}^\circ) + \text{H}^+ \rightarrow (\text{AH}_2/\text{AH}^-) + \text{A}$	$2 \times 10^5$	$2 \times 10^5$	
23	$\text{A}^\circ + \text{O}_2 \rightarrow (\text{AH}^\circ/\text{A}^\circ) + (\text{HO}_2^\circ/\text{O}_2^-)$	$10^2$	$10^2$	

reaction-diffusion mechanisms, than publications that only measure the myoglobin forms at the surface of the meat. Most of the rate constants of our reaction scheme (Table 1) have been measured in literature at 20°C. Therefore, our calculations will be performed at this temperature.

However, it will be possible to use the reaction-diffusion model under practical storage conditions adding Arrhenius type laws.

## 2. Material and methods

This chapter presents the equations of the reaction-diffusion model, the rate constants introduced in the model, the boundary conditions and the numerically methods used to solve the system of equations, and the sensitivity analysis strategy. The material and methods used by Saenz et al. (2008) are not described here since they can be found in their publication.

### 2.1. Mathematical model and numerical procedures

The model has been restricted to one dimension, a single meat compartment geometry, and considering the assumptions summarized in Table 2.

The reactions system of equations to be solved can be written as follows:

$$\frac{d[C_i]}{dt} = \sum_{j=1}^N a_{ij} k_j \left( \prod_{i \in [1,M], a_{ij} < 0} [C_i]^{-a_{ij}} \right)$$

For dioxygen specifically, diffusion is also considered, hence the equation becomes the following:

$$\frac{\partial [O_2]}{\partial t} = D \frac{\partial^2 [O_2]}{\partial x^2} + \sum_{j=1}^N a_{ij} k_j \left( \prod_{i \in [1,M], a_{ij} < 0} [C_i]^{-a_{ij}} \right)$$

where  $C_i$  is concentration of compound  $i$ ,  $k_j$  is the reaction rate constant of reaction  $j$ ,  $a_{ij}$  is the stoichiometric coefficient of compound  $i$  in reaction  $j$ .  $a_{ij}$  is positive if the compound is a product, negative if it is a reactant, and zero if the compound does not participate in the reaction.  $M$  is the number of compounds and  $N$  the number of reactions in the chemical system.  $D$  is oxygen diffusivity.

An algorithm was developed that make it possible to consider: (1) a large number of reactions, (2) variations of different magnitudes in the different terms of the system of equations connected to the diffusion or to the rate constants of the reactions. A robust numerical model, written in MATLAB, was used to solve the reaction-diffusion system of equations. The resolution of this system included two loops. The first loop solves the diffusion of oxygen into the muscle tissue by discretizing the diffusion equation using a second-order Crank–Nicolson finite difference method that has the advantage of being numerically stable and accurate (Özışık, 1994; Kondjoyan et al., 2006a, Kondjoyan et al., 2006b). At

each time-step, the reaction system made up of ordinary differential equations was solved only in the numerical meshes where the oxygen had actually diffused. The algorithm used to solve the ordinary differential equations was the MATLAB ode15s solver. This solver applies to stiff systems, which was important in our case because of the order-of-magnitude differences in the rate constants of the different chemical reactions. The model was applied on an infinite flat plate geometry of 2 cm thickness (one-dimensional geometry). A Dirichlet boundary condition was used at the meat surface exposed to oxygen, with oxygen concentration being that of the oxygen-soluble content in the meat at the given temperature and packaging oxygen content. An Excel interface was used to easily change the group of reactions and rate constants considered. To test the impact of numerical meshing on the results, we ran a set of preliminary calculations using 80, 100, 200 or 400 meshes. The time needed for the MATLAB code to simulate an 8-h period in storage at 20°C on a desktop PC (Windows 10, Intel® Core™ i7-4790S 3.2GHz CPU) was 11 min, 18 min, 4 h, and 18 h for 80, 100, 200 and 400 meshes, respectively. The average difference between the 400-mesh solution and the 200-mesh solution over the first 0.5 mm from the surface was 5% of the 400-mesh solution for MbO<sub>2</sub> and 8% for MMB. These differences became 8% and 14% when the 100-mesh solution was compared to the 400-mesh solution. These differences were mainly localized in the first mesh at the surface of the meat. The spatial locations of the maximum and minimum values in the MbO<sub>2</sub> and MMB profiles were slightly affected by refining the mesh, especially when using a 200-mesh resolution. We thus used 100 meshes for a first assessment of model parameters, and then 200 meshes for the later final determination of the model parameters and the comparison with experimental results.

### 2.2. Initial determination of the rate constants values

**Table 1** lists the initial rate constants of the different reactions at pH 5.5 and 20°C and their literature references. The values of the equilibrium association-constant ( $k_3/k_2$ ) found in the literature varies from  $10^5$  (Richards, 2013) to  $0.8 \times 10^6$  (Tofteskov et al., 2017). The constant introduced by Tofteskov et al. (2017) in their model is  $1.00 \times 10^6$  but its possible range of variation of  $k_3$  is wider (from  $2.00 \times 10^5$  to  $4.00 \times 10^8$ ). In the second route of formation of DMb, our initial rate constant values of  $k_4$ ,  $k_5$  and  $k_6$  were those estimated by Tofteskov et al. (2017) based on analysis of Brantley et al. (1993)'s results. As the N value was not specified, it was allowed to vary from 1 to 45 mol·L<sup>-1</sup> (water in meat tissue). As we found no reaction rate values for the reactions 7 to 9, an experimental study (not detailed here) was conducted in our laboratory using the detection methods developed by Gatellier et al. (1995) and found that the reaction rate of reactions 7 or 8 was much greater than 9, leading to the estimated rate constant values given in **Table 1**. Considering all the biochemical reactions of respiration would have required us to compartmentalize the geometry of the model between the cytosol and all the mitochondria, which was beyond the scope of this paper. Thus, the balance of the respiration reaction was written as reaction 10 in **Table 1**, assuming that all the coenzymes involved in pyruvate formation, the TCA cycle, and the mitochondrial electron transport chain were in non-limiting quantities. **Table 3** presents OCR values measured by several authors at room temperature and at a pH of 5.6. This data selected from the literature was measured without additional reactants or enzymes in the case of meat tissues, or with a little substrate and no added ADP in the case of extracted mitochondria. The measurements obtained on isolated mitochondria are consistent across studies, and vary from 30 to  $40 \times 10^{-9}$  mol of O<sub>2</sub> consumed per mg of mitochondria and per minute at the exit of the slaughterhouse to  $25\text{--}30 \times 10^{-9}$  mol of O<sub>2</sub> 3–4 days later and then to  $15\text{--}20 \times 10^{-9}$  mol of O<sub>2</sub> beyond 7 days in storage. The rate of mitochondrial extraction from skeletal-muscle meat (Ke et al., 2017) can be used to transpose OCR measurements on mitochondria to muscle tissues. These values can then be compared to those measured directly on beef heart muscle (Tang et al., 2005). The values

**Table 2**  
Main assumptions made to build our reaction-diffusion model.

Mechanisms/Reactions	Assumption	Reason
Diffusion	Only oxygen diffuses in meat	Dissolved gas diffuses much more rapidly than other compounds
Reactions of water-soluble compounds	Occur in cytosol of skeletal muscle cells	Myoglobin is in the cytosol
Reactions of lipid compounds and reactions with the vitamin E	Not considered in the paper	Require 2D modelling and compartmentalization of lipids, from the meat piece scale to the cell membrane scale
MMb reduction via the enzymatic NADH-dependent metmyoglobin reductase pathway and the mitochondrial electron transport chain	Not considered in the paper	Require representation of the transport and of the reactions at mitochondrial scale
Effect of the radicals generated by oxidation on myoglobin degradation	Not considered in the paper	Would have required the prediction of the formation of the radicals from lipid reactions

**Table 3**

Oxygen consumption rates (OCR) measured by different authors on extracted mitochondria or on meat tissue at ambient temperature and at pH 5.6. This data was selected from the literature as it was measured without additional reactants or enzymes in the case of meat tissue or with a little substrate and no added ADP in the case of extracted mitochondria. OCR values for meat were directly measured on the tissue in Tang et al. (2005) but calculated by us from the mitochondrial rates in Ke et al. (2017).

Reference	Muscle used or source of extracted mitochondria	Maturation	Oxygen consumption rate (OCR)				
			pH	T (°C)	O <sub>2</sub> moles (mg mitochondria) <sup>-1</sup> min <sup>-1</sup> × 10 <sup>-9</sup>	Mitochondrial content mg/g <sub>meat</sub>	O <sub>2</sub> moles (g meat) <sup>-1</sup> min <sup>-1</sup> × 10 <sup>-9</sup>
Cheah and Cheah (1971)	Beef heart muscle	60 days	5.6		22.4		
	LL	Day 0	5.6	25	30.2	0.21	3.0
	LL	Day 3			26.5	0.19	5.0
Ke et al. (2017)	LL	Day 7			22.4	0.15	3.4
	PM	Day 0			42.5	0.38	16.2
	PM	Day 3			32.4	0.24	7.8
	PM	Day 7			15.2	0.12	1.8
Tang et al. (2005)	Heart beef muscle	2 h30	5.6	25	40.0		0.41
		4 days	without added ATP		24.9		0.29
		60 days			22.4		0.06

calculated on longissimus lumborum (LL) and Psoas major (PM) are about ten times greater than the values measured on beef heart muscle. Since this study is mainly focused on meat from skeletal muscle, we chose to use the data in Ke et al. (2017) to assess the rate constant of the respiration reaction. The rate of this reaction theoretically depends not only on the concentration of O<sub>2</sub> but also on the concentration of the other reactants (glucose, ADP, PO<sub>4</sub>H<sup>+</sup>), at orders that will almost certainly differ from the stoichiometric numbers because reaction 10 is not an elementary reaction but a balance reaction. Since the time-course variations in concentration of these reactants are not known, we decided to simplify the calculation of the reaction rate by considering only the O<sub>2</sub> concentration and introducing an apparent rate constant value that depends on the reaction order chosen. It was found (Ke et al., 2017) that k<sub>10</sub> ≈ 0.3 to 1.8 × 10<sup>-5</sup> mol O<sub>2</sub> consumed per kilogram and per second if we use a first-order reaction (with [O<sub>2</sub>] ≈ 2.5 × 10<sup>-4</sup> mol·L<sup>-1</sup>). However, these rate constant values were measured during quite short periods using mitochondria supplemented with substrate, whereas in meat, the concentration of reactants and substrate are likely to decrease during aging. It is therefore reasonable to extend the range of variation of k<sub>10</sub> towards lower rate constant values than those calculated above.

This leads us to propose a range of O<sub>2</sub> consumption of 10<sup>-7</sup> to 10<sup>-5</sup> mol·L<sup>-1</sup>·s<sup>-1</sup> if the reaction is first-order. Tofteskov et al. (2017) began their numerical simulations with a k<sub>10</sub> value of 2.8 × 10<sup>-3</sup> mol·L<sup>-1</sup>·s<sup>-1</sup> but found better agreement with the experiments of Saenz et al. (2008) when using a final value that was 10 times higher. This final value of Tofteskov et al. (2017) is more than thousand times greater than 10<sup>-5</sup> mol·L<sup>-1</sup>·s<sup>-1</sup>. We have thus widened the range of O<sub>2</sub> consumption due to mitochondrial respiration up to 10<sup>-2</sup> mol·L<sup>-1</sup>·s<sup>-1</sup>, even if the rate constant value found by Tofteskov et al. (2017) almost certainly masks problems related to the underestimation of oxygen consumption by other reactions than respiration. The production of H<sub>2</sub>O<sub>2</sub> in white meat has been estimated (Harel & Kanner, 1985) as 1.25 × 10<sup>-8</sup> mol·L<sup>-1</sup>·s<sup>-1</sup> at pH 5.6 and 35°C. We chose to use this value as the starting point for k<sub>11</sub> even though the real value is likely to be higher in beef meat muscles.

### 2.3. Model application on the initial reaction-scheme

As a first modelling stage in the work, some simulations were carried out at homogeneous oxygen concentrations to study the sensitivity of myoglobin oxygenation, and oxidation, to each of the 44 reactions

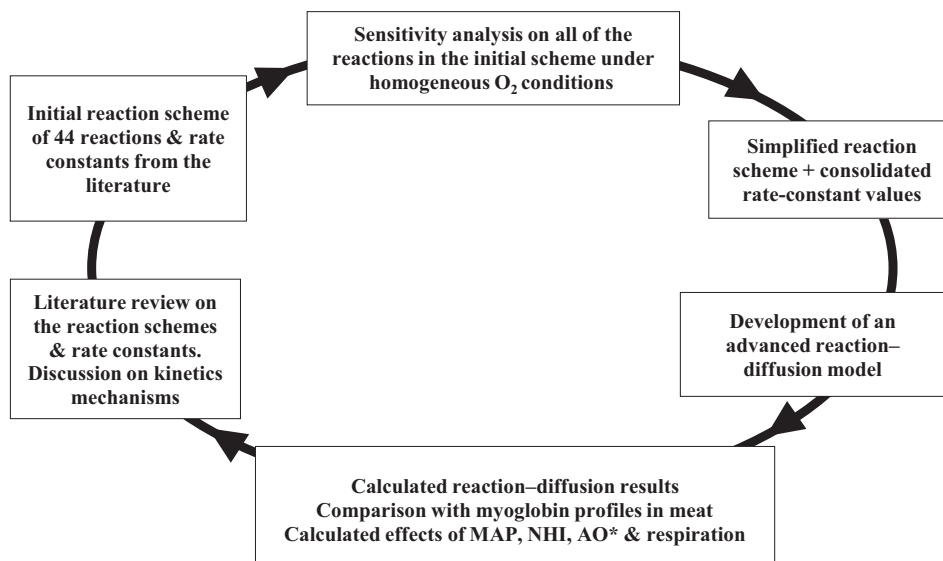


**Fig. 1.** Representation of the approach followed in this paper. \*MAP, NHI and AO refer to modified atmosphere packaging, non-heme iron (Fenton reactions), and water-soluble antioxidants respectively.

making up our initial reaction scheme (Fig. 1). For this first sensitivity analysis, performed using the previously-developed (Oueslati et al., 2018) SIMULOX software, the diffusion term was set to nil and only the rate constants connected to myoglobin reactions were made to vary, as the rate constants of the Fenton chemistry and antioxidant reactions were known from the previous study (Oueslati et al., 2018). The sensitivity calculations were performed using different methods: (1) determination of the contribution of each reaction of the scheme to the rate of formation of the targeted compounds, (2) effect of a variation in the rate constants of the reactions on the formation/consumption of targeted compounds, or (3) removing the studied reactions from the system and looking at the impact on the targeted compounds. The target compounds for the sensitivity analysis were the different forms of myoglobin, oxygen, and hydrogen peroxide. Hydrogen peroxide was considered as a target compound because it is involved in MMb consumption (reaction 8 in Table 1). The sensitivity calculations were performed: (1) by setting the oxygen concentration to a constant value that was either its maximum value in the muscle, or the maximum value divided by 10, or (2) by analyzing the time-course of oxygen consumption driven by the different reactions starting from an initial maximum oxygen concentration value.

After the sensitivity analysis, and to calculate the profiles of myoglobin in the meat, the initial conditions were such as that: the myoglobin was assumed to be in the form of DMb everywhere in the meat, at a concentration of  $4.70 \times 10^{-4}$  mol·L<sup>-1</sup>. Fe<sup>2+</sup> and glucose concentrations were  $2.00 \times 10^{-4}$  mol·L<sup>-1</sup>. H<sup>+</sup> and OH<sup>-</sup> concentration were calculated from the pH of the beef muscle (pH 5.6). Antioxidant concentrations (Oueslati et al., 2018) were superoxide 240 U·ml<sup>-1</sup> dismutase, 640 U·ml<sup>-1</sup> catalase, 20,000 μmol·L<sup>-1</sup> carnosine, 850 μmol·L<sup>-1</sup> glutathione, and 100 μmol·L<sup>-1</sup> ascorbate. The initial concentrations of other compounds were zero.

### 3. Results

Numerical simulation began with sensitivity analysis performed under homogeneous oxygen conditions that enabled us to simplify the 44-reaction scheme (Fig. 1). This simplified reaction scheme was used to compare calculations with the spatial distributions of MbO<sub>2</sub> and MMb measured in a meat cut stored at 20°C under air-permeable packaging conditions. The time-course profiles of percentages of the three major forms of myoglobin measured (Saenz et al., 2008) in a piece of longissimus lumborum (LL) stored at 20°C were used for this comparison. Then, the parameter values that best described the previous experiments were introduced into the reaction-diffusion model to simulate the effects of MAP, Fenton chemistry, water-soluble antioxidant contents, and mitochondrial respiration intensity on the O<sub>2</sub>, H<sub>2</sub>O<sub>2</sub>, MbO<sub>2</sub>, and MMb profiles.

#### 3.1. Sensitivity of model response to the different reactions: Measurements vs calculations

There is not room in this paper to detail all the results obtained in the sensitivity analysis performed under homogeneous oxygen conditions. Only the conclusions of this analysis are given here to focus the paper on the results obtained in meat pieces. The sensitivity analysis on the relative contributions of the reactions to formation/consumption of the target compounds concluded that the Fenton and antioxidant parts of the reaction scheme could be simplified to the reactions 12–23 listed in Table 1. This does not mean that all the Fenton and antioxidant reactions (Oueslati et al., 2018) are in all cases equivalent to reactions 12–23, but that the simplified scheme led to the same results as the complete scheme for the compounds targeted in this study (i.e. the different myoglobin forms, plus oxygen and hydrogen peroxide) and under the boundary conditions considered here. The rate constants of the simplified model and the allied myoglobin reactions were made to vary to study their influence on the formation of the different forms of

myoglobin. The results proved that: (1) the concentration of ferryl-myoglobin was generally very small compared to the concentrations of the three other forms of myoglobin (ferrylmyoglobin was generally less than 1% of the sum of all the myoglobin forms), (2) the contribution of reaction 9 to variation in myoglobin forms was negligible, (3) the effect of reaction 7 was small compared to the effect of reaction 8. It was also observed that in the starting conditions when almost all myoglobin was in the form of DMb, the kinetics of oxygen consumption was mainly driven by reaction 3, as reactions 6 and 10 only had effect on oxygen kinetics in a second stage as they much smaller rate constants than reaction 3. The percentage of MMb formed was dependent on reactions 1 and 6. The reaction scheme borrowed from Brantley et al. (1993) (4–6) was important to simulate the presence of a maximum of MMb under the meat surface. The impact of reaction 4 on MMb formation depends on both k<sub>4</sub> and N, which could not be identified independently. Brantley et al. (1993)'s route have a greater effect on MMb formation than reaction 1 when the rate constant of reaction 6 took the value from the literature ( $k_6 = 5.0 \times 10^{-1}$ ) and when the values of N were greater than 20 mol·L<sup>-1</sup>. Finally, it was concluded that the effect of k<sub>3</sub> and then of the rate constants of reactions 1, 2 and 6 were the other most influential parameters of the model.

Neglecting reaction 9 finally led to a 22-reaction scheme that was equivalent to the initial 44-reaction scheme (Table 1). This simplified 22-reaction scheme was used to simulate the spatial distributions (profiles) of the three major forms of myoglobin in the meat cut. Before comparing calculated and experimental results, we first verified that the 44-reaction scheme led to the same results as the 22-reaction scheme in meat when the input conditions of experiments (Saenz et al., 2008) were introduced in the reaction-diffusion model, whatever the rate constant values chosen in reported ranges of variation (Table 1).

#### 3.2. Influence of the rate constants on calculated MbO<sub>2</sub> and MMb profiles and agreement with measured profiles

Since reaction 3 had the greatest influence on the near-surface proportions of MbO<sub>2</sub> and MMb calculated by the model, we first studied the effect of k<sub>3</sub> before determining the set of parameters that best describes the results of Saenz et al. (2008). The color lines in Fig. 2 present the MbO<sub>2</sub> and MMb profiles calculated for different values of k<sub>3</sub> and compared to the measurements (Saenz et al., 2008) in a piece of longissimus lumborum (LL) muscle stored under an oxygen-permeable film at 20°C for 2 h (Fig. 2a), 4 h (Fig. 2b) and 8 h (Fig. 2c); measurements at 6 h are not given as they shared a near-identical time-course to measurements at 4 h. The experimental value for the near-surface area (diamonds symbols in Fig. 2) show that after 2 h of storage, DMb was mainly replaced by MbO<sub>2</sub> and MMb. The maxima of MbO<sub>2</sub> and MMb were both localized almost at the surface, where MbO<sub>2</sub> was the predominant form at this timepoint (Fig. 2a). After 4 h, the experimental value of MMb increased up to 65% at the surface, while the maximum MMb value was still at less than 1 mm from the surface. Conversely, the experimental value of MbO<sub>2</sub> decreased to less than 20% at the surface, while the maximum MbO<sub>2</sub> value had shifted to about 2 mm away from the surface. This shift translated into a rounder MbO<sub>2</sub> profile in the meat, thus giving the curve a specific recognizable shape. The evolution of these MbO<sub>2</sub> and MMb spatial distributions continued up to 8 h of storage, leading to fairly narrow MMb peak localized close to the surface, while the value of MbO<sub>2</sub> became almost nil at the surface without losing the recognizable shape of its profile which peaked at 20% at 2 mm from the surface.

In the calculated results, peak MbO<sub>2</sub> was always localized at the surface of the meat, whatever the storage period. When k<sub>3</sub> was greater than  $7 \times 10^7$ , the calculations led to a sub-peak in the MbO<sub>2</sub> profile located at 2–2.5 mm from the surface. k<sub>3</sub> values greater than  $7 \times 10^7$  also reproduced the recognizable shape of the MbO<sub>2</sub> profile observed experimentally. Model simulations also reproduced the experimentally-observed peak of MMb when using the rate constant values proposed in

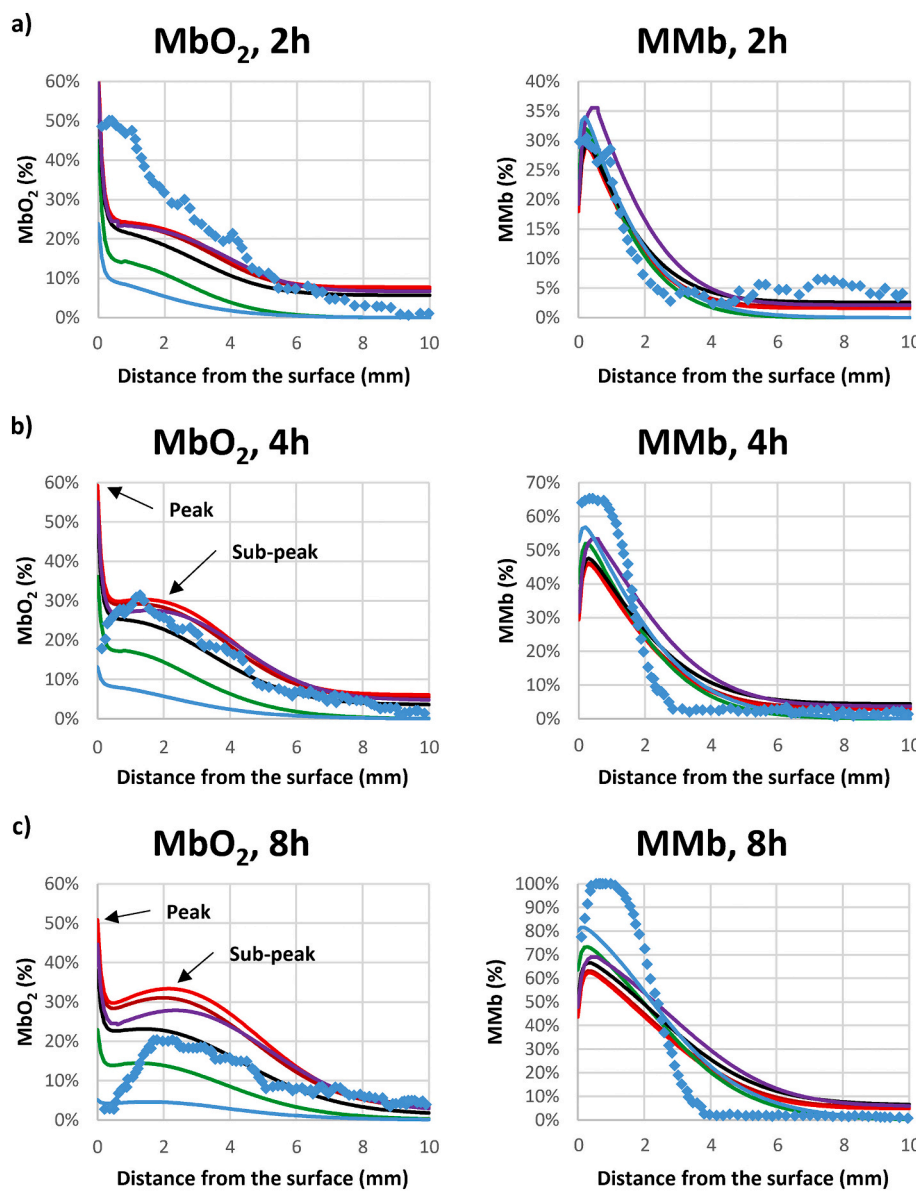


**Fig. 2.** Effect of the rate constant of reaction 3 on the spatial distributions of  $\text{MbO}_2$  and  $\text{MMb}$  in the meat after 2 h (a), 4 h (b) and 8 h (c) in storage at 20°C. Comparison with measured values reported in Saenz et al. (2008) (plotted as blue diamonds). Lines are the results of the model using different rate-constant values for reaction 3, i.e.  $k_3$  is:  $6 \times 10^7$  (in blue),  $2 \times 10^8$  (in green),  $4 \times 10^8$  (in black),  $6 \times 10^8$  (in purple),  $8 \times 10^8$  (in brown), and  $1 \times 10^9$  (in red). (For interpretation of the references to color in this figure legend, the reader is referred to the web version of this article.)

**Table 1** for the reactions 1, 2, 4, 5, and 6. However, beyond 2 h of storage, model calculations underestimated the  $\text{MMb}$  value measured at the peak. Moreover, it became impossible to simulate the experimentally-observed decrease of  $\text{MbO}_2$  at the meat surface after 4 h and 8 h of storage, whatever the rate constants used in the model. We therefore continued the calculations to determine whether the experimental results of  $\text{MMb}$  and  $\text{MbO}_2$  close to the surface could be better reproduced for longer storage times. More than 16 h of storage were needed to have a similar  $\text{MMb}$  peak value in the calculations as in the measurements. The  $\text{MbO}_2$  value calculated at the surface after 16 h in storage was also nil. However, the predicted value of the sub-peak of  $\text{MbO}_2$  was only about 2%, which was not coherent with the measured value of 20% (Saenz et al., 2008) (see Fig. 2). The modelled  $\text{MMb}$  peak was always a little bit narrower than the measured  $\text{MMb}$  peak, whatever the rate constants introduced in the model. Part of these differences in the zone close to the meat surface can be explained by measurement uncertainties, which can be assessed calculating the deviation to 100% of the sum of the three forms of myoglobin as a function of distance to the surface. After 2 h of storage (Table 4), the sum of the measurements of the three myoglobin forms was equal to 100% only at about 1 mm from the surface, whereas it was underestimated by 20% at 0.4 mm from

**Table 4**

Difference between the sum of the three myoglobin forms ( $\text{MbO}_2$ ,  $\text{MMb}$  and  $\text{DMb}$ ) measured by Saenz et al. (2008) and 100% after two hours of storage. Results are similar for the other periods in storage.

Distance from the surface (mm)	Difference from the sum of the 3 myoglobin forms to 100%
0.40	-15.3%
0.52	-12.1%
0.70	-11.9%
0.80	-6.2%
0.96	-6.1%
1.13	2.2%
1.26	8.5%
1.36	9.0%
1.48	11.1%
1.78	16.8%
2.18	19.0%
2.39	20.1%
2.77	21.1%
3.31	17.9%
3.50	17.3%
3.78	16.2%

the surface and overestimated by 20% 2 mm from the surface. These deviations are necessarily mainly due to uncertainties, because the sum of the three experimental forms of myoglobin can never have exceeded 100%, and the percentage of ferryl is not enough to explain the deficit in the sum of the myoglobin forms calculated at the meat surface. However, part of the deviation can also be caused by model assumptions and by a lack of reaction scheme mechanisms, as discussed in Section 4.

The above analysis on the effect of  $k_3$  was completed by an analysis of other influential parameters, i.e. the rate constants of the reactions 1, 2, and 6 and the value of N. A function was defined to analyze the deviation between the experimental profiles shown in Fig. 2 and the profiles calculated by the reaction-diffusion model. The deviation function chosen was the sum of the mean square differences of MMb and MbO<sub>2</sub> divided by their average percentages. A term was also added in the function to force the calculated peak of MMb to be under the meat surface. Only MMb and MbO<sub>2</sub> were considered in this analysis, because DMb could be deduced from the concentrations of the two other myoglobin forms, and because DMb was less abundant in the first few millimeters below the surface, where most of the profile variations were observed. The intervals considered for the studied parameters were  $6 \times 10^7 \leq k_3 \leq 10^9$ ,  $10^{-9} \leq k_{10} \leq 10^{-3}$ ,  $10^{-9} \leq k_{11} \leq 10^{-7}$ , and  $1 \leq N \leq 9$ . The analysis proved that the minimum of the model-experiment deviation was located in the following range of variation in the parameters:  $8 \times 10^7 \leq k_3 \leq 4 \times 10^8$ ,  $10^{-9} \leq k_{10} \leq 10^{-5}$ ;  $10^{-9} \leq k_{11} \leq 10^{-7}$ ;  $2 \leq N \leq 3$ . Two sets of parameters were found to minimize of the deviation function. In both cases,  $k_{10}$  and  $k_{11}$  were  $10^{-7}$  while the pairs of  $k_3$  and N values were either  $k_3 = 10^8$  and  $N = 2$  or  $k_3 = 2 \times 10^8$  and  $N = 3$ . The  $k_3$  values in both of these pairs were much greater than the initial value introduced in the model from Toftekov et al. (2017). Note that the persistence of a sub-peak in the MbO<sub>2</sub> profile even after 8 h of storage (persistence of a bright red color inside the product) and the increase in meat-surface MMb concentration with time (browning under surface; Fig. 2c) explains why the brown sublayer visually migrates towards the meat surface over time, as observed in practice (Ramanathan et al., 2020).

The pairs of  $k_3$  and N values that minimize the deviation function were introduced in the reaction-diffusion model to numerically simulate the effects of MAP, Fenton chemistry, water-soluble antioxidant contents and mitochondrial respiration intensity on the profiles of O<sub>2</sub>, H<sub>2</sub>O<sub>2</sub>, MbO<sub>2</sub>, and MMb.

### 3.3. Impact of modified-atmosphere packaging (MAP) on MbO<sub>2</sub> and MMb profiles

MAP aims to extend the shelf-life of meat by increasing the percentage of CO<sub>2</sub> in the atmosphere surrounding the product in order to slow down microorganism growth while increasing the percentage of O<sub>2</sub> to preserve the bright red color of beef meat for as long as possible. Temperature during the calculations was 20°C, as the goal was to

analyze the phenomena related to the increase of oxygen content in the packaging atmosphere, and not to predict the time-course of the evolution of myoglobin state under real-life practice conditions, where the temperature ranges most often from 0°C to 4°C. It was also assumed that microorganisms did not affect the myoglobin oxidation (as microbial growth under MAP was inhibited by the presence of CO<sub>2</sub>). Fig. 3a and b chart the effect of an increase in oxygen content in the packaging atmosphere on MbO<sub>2</sub> and MMb profiles calculated in the meat after 2 h and 8 h of storage at 20°C. More oxygen inside the packaging increased the percentage of MbO<sub>2</sub> at the meat surface, but also increased the height of the maximum MMb value just below the meat surface. The increase in oxygen content also led to a slight shift in the location of the peak of MMb towards the inside of the meat. After 2 h of storage, the location of the MMb peak shifted to a distance of about 0.3, 0.5, 0.7 and 0.8 mm from the surface for in-MAP oxygen increased to 23%, 40%, 60% and 80%, respectively. Note that this shift is not linear, as stated by Toftekov et al. (2017), but logarithmic, i.e. it is more pronounced when in-MAP oxygen increases from 23% to 40% than for further increases. An important enlargement of the area where MMb is at its maximum accompanies peak shifting. This enlargement is very important after 8 h of storage (Fig. 3b). Our reaction-diffusion model reproduces several phenomena observed in practice. The increase in MAP oxygen content actually favors a bright red color of the meat surface (increase MbO<sub>2</sub> surface content) and a longer shelf-life for meat color acceptance by consumers. However, this increased MAP oxygen content also widens the brown area inside the meat and leads to a situation sometimes observed where after long MAP storage periods, there is still a bright red surface color covering a thick brown meat cut inside.

It was also shown that after 8 h of storage, increasing the O<sub>2</sub> content in the packaging from 23% to 60% almost reverses the proportion of MbO<sub>2</sub> and MMb at the meat surface, whereas any further increase in O<sub>2</sub> content has less effect on MbO<sub>2</sub> and MMb profiles. The O<sub>2</sub> range of 23% to 60% corresponds to typical MAP practice. The effect of a higher proportion of O<sub>2</sub> on meat color and shelf life remains a debated issue in the meat science community (Kim, Huff-Lonergan, Sebranek, & Lonergan, 2010; Lund, Lametsch, Hviid, Jensen, & Skibsted, 2007).

### 3.4. Effect of Fenton chemistry, antioxidants, and mitochondrial oxygen consumption on myoglobin state

#### 3.4.1. Effect of Fenton chemistry and water-soluble antioxidants

One of the benefits of the model is that it can separate the effects connected with non-heme iron (Fenton) reactions from the effects connected to antioxidant reactions, which in practice are very difficult to vary independently in meat tissues. Fig. 4 presents the effect of different parts of the reaction scheme on MbO<sub>2</sub>, MMb, O<sub>2</sub> and H<sub>2</sub>O<sub>2</sub> profiles in meat after 8 h in storage at 20°C. Time-course changes in the other compounds were also analyzed but are not shown in the figure. Variation in the profiles was analyzed in three steps: (1) first considering only

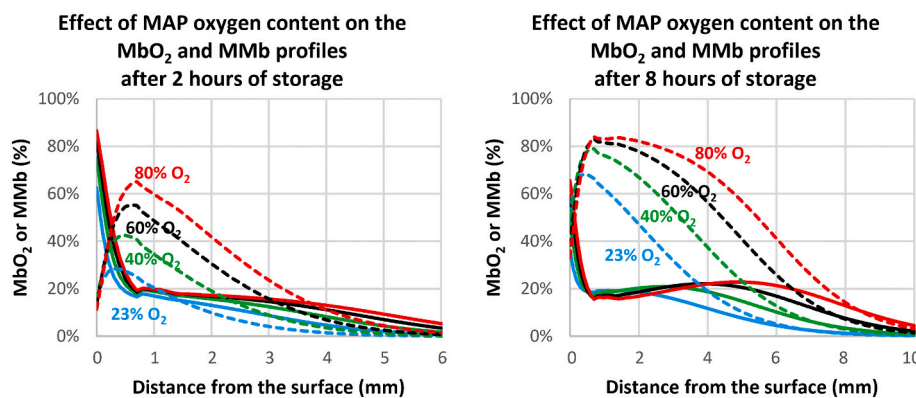


**Fig. 3.** Effect of different oxygen contents under modified-atmosphere packaging (MAP) on the MbO<sub>2</sub> and MMb profiles calculated by the model after 2 h (left) and 8 h (right) in storage at 20°C. Solid lines plot percentages of MbO<sub>2</sub> and dashed lines plot percentages of MMb. Colors show the different MAP oxygen contents, i.e. 23% in blue, 40% in green, 60% in black and 80% in red. (For interpretation of the references to color in this figure legend, the reader is referred to the web version of this article.)

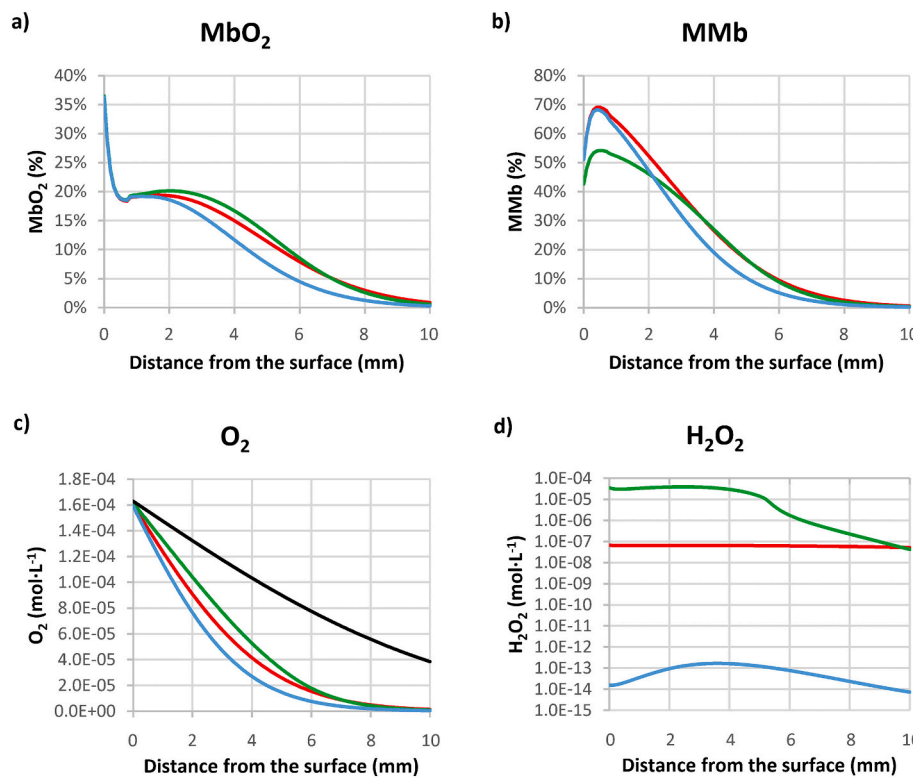


**Fig. 4.** Effect of the different groups of reactions on (a)  $\text{MbO}_2$ , (b)  $\text{MMb}$ , (c)  $\text{O}_2$  and (d)  $\text{H}_2\text{O}_2$  profiles calculated in the meat by the reaction-diffusion model after 8 h in storage at 20°C. Red lines plot reactions that directly involved myoglobin + respiration + formation of  $\text{H}_2\text{O}_2$  from glucose (reactions 1–11 in Table 1); green lines plot these same reactions + Fenton reactions (reactions 1–17 in Table 1); blue lines plot all these reactions + anti-oxidants (reactions 1–23 in Table 3). The black line in Fig. 4c corresponds to the sole effect of diffusion on in-meat oxygen concentration profile. (For interpretation of the references to color in this figure legend, the reader is referred to the web version of this article.)

the group of reactions that directly involve the forms of myoglobin plus mitochondrial respiration and hydroperoxide formation (reactions 1–11, Table 1), (2) then adding Fenton reactions to this group, and (3) then also adding the reactions involving water-soluble antioxidants.

In the group of reactions that directly involve myoglobin, oxygen is used to form either  $\text{MbO}_2$  (reaction 3),  $\text{MMb}$  (reaction 6) or ATP (reaction 10). Oxygen consumption due to these reactions has a major effect on the oxygen profile (Fig. 4c). Adding Fenton reactions to this group leads to more  $\text{H}_2\text{O}_2$  formed (Fig. 4d). This additional  $\text{H}_2\text{O}_2$  leads to a decrease in the peak of the  $\text{MMb}$  profile as reaction 8 converts  $\text{MMb}$  into ferrylmyoglobin (Fig. 4b). Oxygen is both formed and consumed by Fenton-scheme reactions 15 and 16, respectively. The calculated results prove that the balance of the Fenton reactions is in favor of additional formation of oxygen, which is almost certainly explained by the formation of  $\text{O}_2$  by reaction 15 from the  $\text{HO}_2^\cdot/\text{O}_2^\cdot$  radicals coming from reaction 1 (Fig. 4c). This leads to a slight increase in the sub-peak in the  $\text{MbO}_2$  profile (Fig. 4a) and a decrease in the peak of  $\text{MMb}$ , which in turn leads to less formation of  $\text{MMb}$  due to Fenton chemistry. That seems to contradict the literature, and is probably explained by some missing mechanisms in the model, as discussed in Section 4. Adding the water-soluble antioxidants to the previous groups of reactions leads to greater consumption of oxygen and  $\text{H}_2\text{O}_2$  inside the meat tissue (Fig. 4c and d). This leads to an increase in peak  $\text{MMb}$  value that returns to its previous level when we used the group of reactions 1–11 that directly involve the myoglobin forms. However, the presence of antioxidants led to a sharper decrease in  $\text{MMb}$  from the peak and towards the inside of the sample (Fig. 4b). Likewise, the decrease in the  $\text{MbO}_2$  profile from its sub-peak and towards the inside of the sample was also more pronounced with the antioxidants than without them (Fig. 4a).

#### 3.4.2. Effect of oxygen consumption rate due to mitochondrial respiration

In previous calculations (Fig. 2), the rate constant of mitochondrial respiration ( $k_{10}$ ) was by default set to  $10^{-7}$  in a first-order reaction. This default value corresponds to the average of the measurements found in the literature (Table 3). However, much larger values, of the order of  $10^{-3}$  to  $10^{-2}$ , have been considered (Tofteskov et al., 2017). We

therefore analyzed the effect of varying OCR between  $10^{-8}$  and  $10^{-2}$  on the  $\text{MbO}_2$  and  $\text{MMb}$  profiles of meat in storage for 8 h at 20°C. There was no effect when  $k_{10}$  ranged between  $10^{-8}$  and  $10^{-5}$ , whereas the increase of the respiration rate constant resulted in a large increase in  $\text{O}_2$  consumption when  $k_{10}$  ranged between  $10^{-5}$  and  $10^{-2}$  (Fig. 5, right). This additional  $\text{O}_2$  consumption resulted in a decrease in the percentages of  $\text{MbO}_2$  and  $\text{MMb}$  formed at the surface of the meat, particularly after more than 4 h in storage (Fig. 5, left). As  $\text{MbO}_2$  and  $\text{MMb}$  decreased simultaneously, their ratio at the meat surface was less changed. There was a different pattern inside the meat, where the increase of the respiration rate constant resulted in a much faster decrease in  $\text{MbO}_2$  value as a function of distance from the surface, as well as a shift in location of the  $\text{MMb}$  peak towards this surface. This combination of a decrease in  $\text{MbO}_2$  with a shift in  $\text{MMb}$  peak towards the surface could contribute to the color instabilities observed in practice on meat muscles undergoing significant and time-varying mitochondrial respiration. However, these variations are only observed for much higher  $k_{10}$  values than those measured in practice. This suggests that the color instabilities due to mitochondrial respiration likely involve additional reactions connected with the mitochondrial electron transport chain and enzymes associated with the Krebs cycle.

#### 4. Discussion on the performances and limits of the model

From a methodological point of view, the approach used in this work enabled us to develop a coupled reaction-diffusion model starting from a complex scheme of reactions involved in the variation of surface quality of a solid food. The resulting model is, to our knowledge, the most complete mathematical description of the evolution of myoglobin state in beef meat to date. Sensitivity analysis led to a simplified 22-reaction scheme that was kinetically equivalent to the initial 44-reaction scheme in terms of the evolution in distributions of  $\text{O}_2$ ,  $\text{H}_2\text{O}_2$  and the different forms of myoglobin inside the meat. The calculated concentration of ferrylmyoglobin was always negligible compared to the three other forms of myoglobin, except when Fenton reactions were added to reactions 1–11 without the meat-soluble antioxidants, which normally

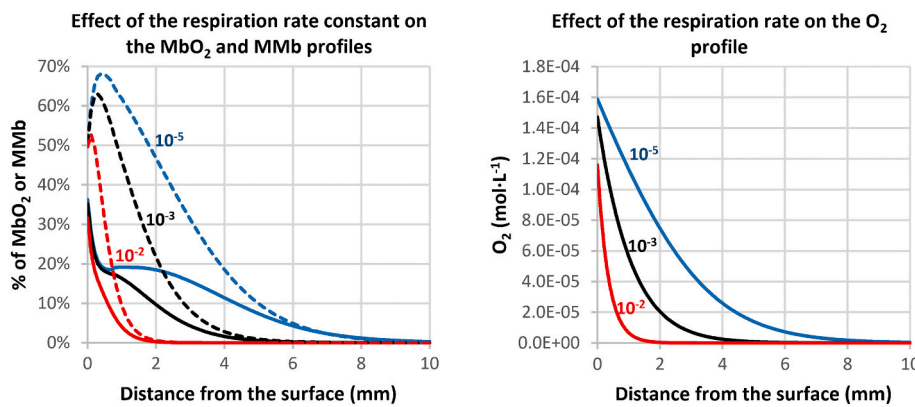


**Fig. 5.** Effect of the mitochondrial respiration rate constant ( $k_{10}$ ) on  $\text{MbO}_2$  (solid lines) and MMB (dashed lines) profiles (left) and on the  $\text{O}_2$  profile (right) over the course of 8 h in storage at 20°C. The  $k_{10}$  values plotted in different color lines are  $10^{-5}$  in blue,  $10^{-3}$  in black and  $10^{-2}$  in red. (For interpretation of the references to color in this figure legend, the reader is referred to the web version of this article.)

never happens in practice (Fig. 4d). Calculated results prove that the model needs to be parameterized with a higher rate constant for reaction 3 (formation of  $\text{MbO}_2$  from DMb) than that proposed previously (Toftekov et al., 2017) in order to predict the recognizable shape of the  $\text{MbO}_2$  profile observed experimentally. Thanks to Brantley et al. (1993)'s reaction route and the introduction of appropriate rate constants in reactions 4–6, the model can also correctly predict the peak of MMB formed under the meat surface and the existence of the brown sublayer observed in practice. The persistence of a secondary sub-peak in the  $\text{MbO}_2$  profile associated with an increasing MMB concentration at the surface of the meat explains the visual migration of the brown sublayer observed in practice. Calculations under MAP conditions also predicted a situation observed where  $\text{MbO}_2$  concentration is still high at the meat surface while a large MMB area develops deeper inside the product, which leads to a red meat surface covering a brown inside area. The model was also used to analyze the respective effects of Fenton reactions, water-soluble antioxidant reactions (superoxide dismutase, catalase, carnosine, glutathione, ascorbate), and mitochondrial respiration-driven oxygen consumption reactions on the evolution of myoglobin state. Results illustrate: (1) how oxygen consumption rate can contribute to color instabilities observed in practice on meat muscles undergoing significant and time-varying mitochondrial respiration, and (2) how the presence of water-soluble antioxidants can offset the effect of Fenton chemistry on the shape of the  $\text{MbO}_2$  and MMB profiles. However, the reaction scheme presented here, which is focused on the effects of  $\text{O}_2$  and  $\text{H}_2\text{O}_2$  on the evolution of the myoglobin state, also leads to unexpected results, such as the decrease in MMB peak connected with the effect of Fenton chemistry. This can be explained by mechanisms missing in the model, which would have required additional modelling work and compartmentalization. For example, the effect of surface microorganisms on oxidation, which is not considered in the model, probably contributes to the differences observed between the experimental and calculated  $\text{MbO}_2$  profiles just under the meat surface for periods of more than 2 h in storage at an ambient temperature of 20°C (Fig. 2b and c). Limiting the effect of mitochondrial respiration to oxygen consumption (reaction 10) was also too reductive. It would have been instructive to account for the MMB reduction that occurs via the enzymatic NADH-dependent metmyoglobin reductase pathway and via the mitochondrial electron transport chain. This would have theoretically required a model that represents all the mitochondrial compartments included in the cytosol. As it is unreasonable to attempt to model all the mitochondria, we could have used approximations, such as designing a single equivalent 'model' mitochondrial compartment that would have exchanged reactants, such as pyruvate, with the cytosol. It is very likely that in this case, the calculated effects of Fenton chemistry and soluble antioxidants on the evolution of the myoglobin state would have been different, as NAD and cytochrome C are known to affect MMB

formation. The effects of Fenton radicals on the degradation of myoglobin and/or the mitochondrial membrane were also not considered in the model. Myoglobin degradation due to free radicals could also have contributed to the differences observed between measured and calculated  $\text{MbO}_2$  profiles just under the meat surface (Fig. 2c and d).

The one-dimensional, single-compartment nature of the model also does not consider the multiscale fat compartments. Combining a 2-dimensional oxygen transfer and the greater solubility of oxygen in fat than in meat would make it possible to numerically simulate the oxidation that occurs near the superficial fat cover or near the fat separations between different muscles. The geometrical introduction of small fat particles in the meat compartment (beef marbling) and lipid oxidations inside these particles would also make it possible to analyze how far fat oxidation can affect the color of the lean meat compartment. However, as was the case with representing the mitochondria, introducing all the fat particles and the reactions that take place in them would not be reasonable from a computing point of view, and so further approximations would be needed. These limitations point to way to further reaction-diffusion modelling efforts that will require a simplified space compartmentalization of the muscle tissue at different scales.

## 5. Conclusion

This paper aimed at analyzing the effect of reaction mechanisms on the kinetics of variation of the state of myoglobin in a piece of meat subjected to different oxygen concentrations. Advanced reaction-diffusion model and numerical procedures were developed to predict the different kinetics using numerous reactions with rate constants of different orders of magnitude. Sensitivity analysis proved that the initial scheme of reactions was equivalent to a simpler scheme of 22-reaction. Results calculated with this scheme were in agreement with the spatial distributions of the different forms of myoglobin measured by Saenz et al. (2008) in a meat cut stored at 20°C. However, very high values of the rate constant of the myoglobin oxygenation reaction (reaction 3, Table 1) had to be considered to predict correctly the distribution of  $\text{MbO}_2$  near the meat surface. Our reaction-diffusion model was also able to reproduce several phenomena observed in practice when using MAP, or color instabilities phenomena observed on muscles undergoing significant and time-varying mitochondrial respiration. However, the model remains limited due to its background assumptions (Table 2). Multiscale and multi-compartments modelling would probably be required to go further on the study of mechanisms. The model also only predicts the variations of myoglobin at 20°C while meat is stored at temperatures ranging from 0°C to 8°C. Therefore, the present system of equations will have to be completed with Arrhenius type relations and their proper parameter values to predict the variations of myoglobin under practical conditions.

## CRediT authorship contribution statement

**A. Kondjoyan:** Conceptualization, Methodology, Investigation, Supervision, Writing – original draft, Writing – review & editing, Project administration, Funding acquisition. **J. Sicard:** Methodology, Software, Validation, Writing – original draft, Writing – review & editing. **M. Badaroux:** Software, Validation, Formal analysis. **P. Gatellier:** Conceptualization, Investigation, Supervision.

## Declaration of Competing Interest

- This research respects ethical guidelines of Elsevier
- This manuscript has not been published and is not under consideration for publication elsewhere.
- We have no conflicts of interest to disclose

## Acknowledgments

The authors thank Mathematics and Computer Science Master's-course students Benoit Albert, Adélaïde Herriau, Roxane Deflandre, and Hiba Elhayel for their contributions to developing the reaction-diffusion model and identifying its rate constants. The authors also thank the UMT NEWCARN for providing grants to some of these students.

## References

- Brantley, R., Smerdon, S., Wilkinson, A., Singleton, E., & Olson, J. (1993). The mechanism of autoxidation of myoglobin. *Journal of Biological Chemistry*, 268(10), 6995–7010. [https://doi.org/10.1016/S0021-9258\(18\)53138-0](https://doi.org/10.1016/S0021-9258(18)53138-0)
- Cheah, K. S., & Cheah, A. M. (1971). Post-mortem changes in structure and function of ox muscle mitochondria. I. Electron microscopic and polarographic investigations. *Journal of Bioenergetics*, 2(2), 85–92. <https://doi.org/10.1007/BF01648923>
- Cucci, P., N'Gatta, A. C. K., Sanguansuk, S., Lebert, A., & Audonnet, F. (2020). Relationship between color and redox potential (E-h) in beef meat juice. Validation on beef meat. *Applied Sciences*, 10(9), 3164–3177. <https://doi.org/10.3390/app10093164>
- England, E. M., Matarneh, S. K., Mitacek, R. M., Abraham, A., Ramanathan, R., Wicks, J. C., ... Gerrard, D. E. (2018). Presence of oxygen and mitochondria in skeletal muscle early postmortem. *Meat Science*, 139, 97–106. <https://doi.org/10.1016/j.meatsci.2017.12.008>
- Eriksson, M., Strid, I., & Hansson, P.-A. (2014). Waste of organic and conventional meat and dairy products-A case study from Swedish retail. *Resources Conservation and Recycling*, 83, 44–52. <https://doi.org/10.1016/j.resconrec.2013.11.011>
- Gatellier, P., Anton, M., & Renerre, M. (1995). Lipid-peroxidation induced by H<sub>2</sub>O<sub>2</sub>-activated metmyoglobin and detection of a myoglobin-derived radical. *Journal of Agricultural and Food Chemistry*, 43(3), 651–656. <https://doi.org/10.1021/jf00051a018>
- Harel, S., & Kanner, J. (1985). Hydrogen peroxide generation in ground muscle tissues. *Journal of Agricultural and Food Chemistry*, 33(6), 1186–1188. <https://doi.org/10.1021/jf00066a041>
- Ke, Y., Mitacek, R. M., Abraham, A., Mafi, G. G., VanOverbeke, D. L., DeSilva, U., & Ramanathan, R. (2017). Effects of muscle-specific oxidative stress on cytochrome c release and oxidation-reduction potential properties. *Journal of Agricultural and Food Chemistry*, 65(35), 7749–7755. <https://doi.org/10.1021/acs.jafc.7b01735>
- Kim, Y. H., Huff-Lonergan, E., Sebranek, J. G., & Lonergan, S. M. (2010). High-oxygen modified atmosphere packaging system induces lipid and myoglobin oxidation and protein polymerization. *Meat Science*, 85(4), 759–767. <https://doi.org/10.1016/j.meatsci.2010.04.001>
- Kondjoyan, A., McCann, M. S., Rouaud, O., Havet, M., Foster, A. M., Swain, M., & Daudin, J. D. (2006a). Modelling coupled heat-water transfers during a decontamination treatment of the surface of solid food products by a jet of hot air—II. Validations of product surface temperature and water activity under fast transient air temperature conditions. *Journal of Food Engineering*, 76(1), 63–69. <https://doi.org/10.1016/j.jfoodeng.2005.05.015>
- Kondjoyan, A., Rouaud, O., McCann, M. S., Havet, M., Foster, A., Swain, M., & Daudin, J. D. (2006b). Modelling coupled heat-water transfers during a decontamination treatment of the surface of solid food products by a jet of hot air. I. Sensitivity analysis of the model and first validations of product surface temperature under constant air temperature conditions. *Journal of Food Engineering*, 76(1), 53–62. <https://doi.org/10.1016/j.jfoodeng.2005.05.014>
- Krzywicki, K. (1979). Assessment of relative content of myoglobin, oxymyoglobin and metmyoglobin at the surface of beef meat. *Meat Science*, 3, 1–10. [https://doi.org/10.1016/0309-1740\(79\)90019-6](https://doi.org/10.1016/0309-1740(79)90019-6)
- Lund, M. N., Lametsch, R., Hviid, M. S., Jensen, O. N., & Skibsted, L. H. (2007). High-oxygen packaging atmosphere influences protein oxidation and tenderness of porcine longissimus dorsi during chill storage. *Meat Science*, 77(3), 295–303. <https://doi.org/10.1016/j.meatsci.2007.03.016>
- Mancini, R. A., Belskie, K., Suman, S. P., & Ramanathan, R. (2018). Muscle-specific mitochondrial functionality and its influence on fresh beef color stability. *Journal of Food Science*, 83(8), 2077–2082. <https://doi.org/10.1111/1750-3841.14219>
- Oueslati, K., Promeyrat, A., Gatellier, P., Daudin, J.-D., & Kondjoyan, A. (2018). Stoichiokinetic modeling of Fenton chemistry in a meat-nimetic aqueous-phase medium. *Journal of Agricultural and Food Chemistry*, 66(23), 5892–5900. <https://doi.org/10.1021/acs.jafc.7b06007>
- Özışık, M. N. (1994). Crank-Nicholson method. In *Finite difference methods in heat transfer* (pp. 118–121). Boca Raton, Florida: CRC Press.
- Ramanathan, R., Hunt, M. C., Mancini, R. A., Nair, M. N., Denzer, M. L., Suman, S. P., & Mafi, G. G. (2020). Recent updates in meat color research: Integrating traditional and high-throughput approaches. *Meat and Muscle Biology*, 4(2), 1–24. <https://doi.org/10.22175/mmb.9598>
- Ramanathan, R., & Mancini, R. A. (2018). Role of mitochondria in beef color: A review. *Meat and Muscle Biology*, 2(1), 309–320. <https://doi.org/10.22175/mmb2018.05.0013>
- Renerre, M., & Labas, R. (1987). Biochemical factors influencing metmyoglobin formation in beef muscles. *Meat Science*, 19(2), 151–165. [https://doi.org/10.1016/0309-1740\(87\)90020-9](https://doi.org/10.1016/0309-1740(87)90020-9)
- Richards, M. P. (2013). Redox reactions of myoglobin. *Antioxidants & Redox Signaling*, 18(17), 2342–2351. <https://doi.org/10.1089/ars.2012.4887>
- Saenz, C., Hernandez, B., Alberdi, C., Alfonso, S., & Manuel Dineiro, J. (2008). A multispectral imaging technique to determine concentration profiles of myoglobin derivatives during meat oxygenation. *European Food Research and Technology*, 227(5), 1329–1338. <https://doi.org/10.1007/s00217-008-0848-4>
- Stewart, M. R., Zipser, M. W., & Watts, B. M. (1965). The use of reflectance spectrophotometry for the assay of raw meat pigments. *Journal of Food Science*, 30, 464–469. <https://doi.org/10.1111/j.1365-2621.1965.tb01787.x>
- Tang, J. L., Faustman, C., & Hoagland, T. A. (2004). Krzywicki revisited: Equations for spectrophotometric determination of myoglobin redox forms in aqueous meat extracts. *Journal of Food Science*, 69(9), 717–720. <https://doi.org/10.1111/j.1365-2621.2004.tb09922.x>
- Tang, J. L., Faustman, C., Hoagland, T. A., Mancini, R. A., Seyfert, M., & Hunt, M. C. (2005). Postmortem oxygen consumption by mitochondria and its effects on myoglobin form and stability. *Journal of Agricultural and Food Chemistry*, 53(4), 1223–1230. <https://doi.org/10.1021/jf0486460>
- Tofteskov, J., Hansen, J. S., & Bailey, N. P. (2017). Modelling the autoxidation of myoglobin in fresh meat under modified atmosphere packing conditions. *Journal of Food Engineering*, 214, 129–136. <https://doi.org/10.1016/j.jfoodeng.2017.06.002>